https://doi.org/10.1038/s44454-026-00043-3

A PBK model for PFAS transfer from feed to fillet in farmed Atlantic salmon

Tu-Ky Ly[1,2], Cathrin Veenas[3], Cleo Bodin[1,2], Kai K. Lie[3], Rémy Beaudouin[1,2] ✉ & Marc H. G. Berntssen[3]

Despite the establishment of maximum limits for per- and polyfluoroalkyl substances (PFAS) in seafood, no equivalent limits exist for PFAS in fish feed—the primary contamination route in aquaculture. We conducted controlled feeding experiments with Atlantic salmon (*Salmo salar*), exposing fish to six PFAS congeners (PFOS, PFOA, PFNA, PFHxS, PFDA, and PFBS) for 70 days followed by a 56-day depuration phase. Toxicokinetic data were collected across ten tissues, including bile. These data were used to develop a physiologically based kinetic (PBK) model incorporating a dynamic energy budget sub-model for salmon growth dynamics, using a Bayesian inference framework. The model accurately reproduced PFAS kinetics across all tissues and was externally validated against EFSA commercial surveillance data. Simulations indicate that current feed contamination levels pose low dietary PFAS exposure risk and enable direct estimation of maximum acceptable PFAS concentrations in feed relative to established food safety limits. This model provides the first species-specific tool for deriving PFAS feed guidance values for Atlantic salmon, directly supporting regulatory decision-making.

Per- and polyfluoroalkyl substances (PFAS) are a class of synthetic organofluorine compounds extensively employed in industrial and commercial applications, including foams for fire suppression, surfactants, and fluorinated polymers[1]. Due to decades of widespread use, PFAS are now ubiquitous in aquatic environments, and long-chain perfluoroalkyl carboxylic acids can bioaccumulate in protein-rich tissues of marine organisms, including fish[2,3]. Seafood is an important source of human PFAS exposure[4,5], and parts of the European population already exceed the tolerable weekly intake established for selected PFAS[6,7]. PFAS exposure is associated with harmful effects such as altered cholesterol levels[4,8,9], liver damage[4,10,11], developmental disorders[4,12], and most critically, impaired immune function[4,13]. In response, the European Food Safety Authority (EFSA) assessed the risks associated with human exposure to four PFAS of major food safety concern—perfluorooctane sulfonic acid (PFOS), perfluorooctanoic acid (PFOA), perfluorononanoic acid (PFNA), and perfluorohexane sulfonic acid (PFHxS), collectively referred to as the 4-EFSA-PFAS—and maximum limits (ML) have been established for these compounds in food products, including seafood[4,6,7].

Assessing feed-to-food transfer is essential to link contaminant levels in feed with levels in the edible parts of food-producing animals, and this information is necessary to define feed ML compatible with those already established for food. Despite ML now being in force for PFAS in seafood, no equivalent limits have been set for PFAS in feed for any food-producing animals—including fish. The European Commission (EC) has nonetheless developed monitoring recommendations covering feed and its ingredients, as well as guidance on assessing and tracking contaminant transfer to edible tissues[14,15]. Atlantic salmon (*Salmo salar*) farming is one of the most important sources of seafood in the EU[16], and salmon feed is a known vehicle of PFAS contamination: wide-scope surveillance of Norwegian commercial salmon feeds has identified PFOS as the predominant PFAS, followed by PFNA and, to a lesser extent, PFOA[17]. PFAS transfer is congener- and species-specific, depending on carbon chain length, functional group, and elimination half-life[18–20]. Long-chain perfluorosulfonates such as PFOS are progressively being replaced by shorter-chain alternatives, including PFBS[21], which is assumed to have lower bioaccumulation potential[18], though its kinetic behavior in farmed Atlantic salmon remains poorly characterized.

Physiologically based kinetic (PBK) models are key tools in regulatory risk assessment, providing a quantitative mechanistic framework to predict the time-course of chemical concentrations in organs and body fluids based on absorption, distribution, metabolism, and excretion (ADME) processes in combination with the physiology and anatomy of the organism[22–25]. PBK models are particularly valuable for predicting kinetics in farmed fish, where steady-state tissue concentrations may never be achieved: abiotic and biotic factors—including water temperature and growth dilution—can drastically alter the feed-to-organ concentration ratio[24,26,27]. In open sea cage farming specifically, physiological parameters such as feed intake, fat deposition, and growth rate are strongly dependent on ambient seawater temperature and fish life-stage[28,29]. These aquaculture physiological dynamics have a large impact on feed-derived tissue contaminant levels in farmed Atlantic salmon[30].

[1]New Approaches and Models for Human Health and Environmental Safety, INERIS, Verneuil-en-Halatte, France. [2]UMR-I 02 SEBIO, INERIS, URCA, ULHN, Verneuil-en-Halatte, France. [3]Institute of Marine Research, POB 1870 Nordnes, Bergen, Norway. ✉e-mail: remy.beaudouin@ineris.fr

Despite their clear utility, PBK models for PFAS in fish remain exceptionally rare. Fewer than ten such models have been published globally, and those that exist are constrained in scope in ways that preclude regulatory application to farmed Atlantic salmon. Recently developed PFAS PBK models for chickens and swine have specifically addressed feed-to-food transfer in a food safety context, integrating species-specific toxicokinetics, physiology, and production characteristics[31–34]. To our knowledge, no such feed-to-food transfer PBK model is yet available for farmed seawater fish such as Atlantic salmon. A recently developed PBK model for PFOS in rainbow trout described kinetics following dietary exposure and included multiple elimination pathways[35,36]. This model accounts for physiological and aquaculture conditions, including temperature, feeding regimen, and growth dilution, and can be adapted to species-specific fish physiology[24]. In this model, fish growth is represented by a dynamic energy budget (DEB) sub-model driven by temperature and feeding level[24]. However, none of the existing fish PFAS PBK models cover the 4-EFSA regulated PFAS simultaneously, none was designed for feed-to-fillet transfer, and none has been validated against real-world commercial farming data—leaving a critical gap in the regulatory framework.

The present study addresses this gap. We report novel, extensive toxicokinetic data from a controlled 156-day feeding and depuration experiment in Atlantic salmon exposed to six PFAS congeners, covering both functional groups (three sulfonic acids and three carboxylic acids) and a range of carbon chain lengths: the four PFAS regulated in food (PFOS, PFOA, PFNA, PFHxS), PFDA—which is particularly prevalent in Norwegian Atlantic salmon feeds[17]—and the emerging short-chain PFBS. Our aim was to develop an Atlantic salmon-specific PBK model for these six PFAS, focusing on feed-to-fillet transfer, incorporating the species-specific physiology and growth dynamics of farmed Atlantic salmon from smolt to market size, and accounting for realistic aquaculture conditions. The model was calibrated using Bayesian statistics and externally validated against independent surveillance data, providing a robust tool for scenario-based risk assessment and supporting the development of feed guidance values aligned with existing food ML. Concretely, the model was used to predict the PFAS levels in edible fillet of market-sized farmed salmon when fed the highest observed PFAS contamination in Norwegian commercial salmon feeds, and which levels in feed would exceed the current ML established for food (Fig. 1).

Results

PFAS-specific organ accumulation

Tissue PFAS concentrations measured in control fish, fed with the unspiked basal diet throughout the trial, confirmed that background contamination from the basal feed was negligible and did not meaningfully contribute to tissue concentrations measured in exposed fish. A distinct PFAS distribution was observed among tissues, with the highest dose-corrected PFAS levels in plasma, followed by liver, red blood cells, and red muscle; the lowest levels were found in adipose tissue and fillet (Table 1). In addition to differences in tissue distribution, the accumulation pattern differed among PFAS congeners. Highest dose-corrected levels in salmon fillet were observed for PFOS, followed by PFHxS, PFDA, PFBS, PFNA, and finally PFOA (Table 1).

PFAS accumulation in Atlantic salmon increased with carbon chain length, with higher accumulation for the eight-carbon PFOS compared to the four-carbon PFBS (Table 1). Higher accumulation was also observed for sulfonic acids compared to carboxylic acids of equivalent chain length (Table 1). Specifically, PFOS showed nearly threefold higher accumulation than PFNA, and nearly sevenfold higher accumulation than PFOA across Atlantic salmon tissues (Table 1), despite all three sharing an eight-carbon backbone and differing only in their functional group. PFBS showed a similar accumulation to the longer-chain PFOA.

PBK model development

During the feeding trial, fish weight increased nearly fourfold, from a start weight of 138 ± 21 g to 504 ± 104 g. The DEB sub-model accurately reproduced mean growth trajectories ($R^2 = 0.891$, and RMSE = 38.1 g, Fig. S3) throughout the trial (Fig. 2), enabling the model to account for growth dilution during both exposure and depuration phases. Changes in fat proportion in the fillet over the life cycle were best described by a log-linear relationship between fat fraction and body weight, which avoided overestimation of fat content in larger salmon (Fig. S4).

Sensitivity analysis (SA) of PFAS fillet concentrations revealed that the most influential parameters differed between accumulation and depuration phases (Fig. S5). During the exposure phase, fillet concentrations were primarily driven by the red muscle:blood partition coefficient and by the oral absorption constant K_u. During the depuration phase, the blood:water partition coefficient $PC_{blood:water}$, white muscle:blood partition coefficient, and fecal elimination constant $K_{e,feces}$ became most influential. The blood:water partition coefficient, which governs branchial excretion, was an important driver across both phases (Fig. S5).

Bayesian inference calibration produced convergent MCMC chains and identifiable posterior distributions for nearly all parameters (Tables 2, 3). The sole exception was the permeability coefficient of fat in the fillet (PA_{fat}), which was unidentifiable, consistent with the SA results and the absence of separate fat and muscle fraction measurements in fillet samples (Fig. S5). Overall, the experimental dataset generated in this study provided sufficient information to estimate most model parameters (Tables 2 and 3).

Across all ten tissues and six PFAS congeners, the calibrated model accurately reproduced experimental data during both the bioaccumulation and elimination phases (Figs. S6–S11), with 60.2% of measured data predicted within 1.3-fold, 89.7% within twofold, and 97.8% within fivefold (Fig. 3). For each PFAS, model prediction accuracy within the 2–5-fold range was: 95.2–98.4% for PFOA, 84.4–97.4% for PFNA, 90.1–98.6% for PFDA, 92.1–98.7% for PFBS, 94.0–98.8% for PFHxS, and 83.5–95.3% for PFOS (Fig. 4).

The absorption parameter K_u was consistent across the three carboxylic acids, with increasing carbon chain length (PFOA < PFNA < PFDA) associated with decreasing K_u values (Table 2), indicating slower oral absorption for longer, more lipophilic carboxylic acid analogs. Among sulfonic acids, PFBS showed the highest K_u value, while PFHxS and PFOS showed identical K_u values (Table 3). Fillet concentrations were predicted within a twofold range for 90% of PFNA measurements and 100% of PFOA, PFDA, PFBS, PFHxS, and PFOS measurements (Fig. 3).

According to the model, total excretion of free PFAS occurred approximately 98% via the gills, with 1.8% via feces and 0.2% via bile (Fig. S12). Implementation of enterohepatic reabsorption did not significantly improve model predictions in any tissue, and the no-reabsorption scenario provided the best fit (Fig. S13).

Model evaluation and food safety

Norwegian commercial Atlantic salmon feeds displayed a large variation in 4-EFSA PFAS contamination, with sum 4-EFSA PFAS levels of 0.1–3.8 µg/kg ww[17]. Predicted sum PFAS concentrations in farmed Atlantic salmon fillet were approximately 0.01–0.5 µg/kg ww (Fig. 5), within the range of previously surveyed levels in commercial farmed Atlantic salmon muscle (~0.03–0.31 µg/kg ww; EFSA[4], ref. 37). External validation against the independent surveillance dataset confirmed the model's predictive accuracy: for PFHxS, PFNA, and PFBS, both model predictions and measured fillet concentrations were below the limit of quantification (LOQ), demonstrating qualitative agreement. For PFOA, the predicted concentration was marginally above the LOQ, consistent with near-LOQ measured levels. For PFOS, the only congener with a quantifiable fillet concentration in the surveillance dataset, the model predicted a fillet concentration of 0.130 µg/kg ww at the mean commercial feed exposure (0.73 µg/kg ww). In comparison to the observed maximum fillet concentration of 0.12 µg/kg ww, it represents less than 10% deviation and provides quantitative external validation of the model's most regulatory relevant prediction (Fig. 5; ref. 17). When modeled at the highest observed feed PFAS concentrations, predicted levels for PFHxS and PFNA remained below their respective LOQ, while only PFOA and PFOS were predicted above the LOQ (Fig. 5).

Table 1 | Dose-corrected concentrations (mean ± SD, µg/kg ww) at the end of exposure (day 70) for different organs and main elimination routes in Atlantic salmon fed PFAS-enriched diets for 3 months, in triplicate tanks ($n = 9$)

	PFOA $C_8HF_{15}O_2$ (µg/kg)	PFNA $C_9HF_{17}O_2$ (µg/kg)	PFDA $C_{10}HF_{19}O_2$ (µg/kg)	PFBS $C_4HF_9O_3S$ (µg/kg)	PFHxS $C_6HF_{13}O_3S$ (µg/kg)	PFOS $C_8HF_{17}O_3S$ (µg/kg)
Plasma	127.3 ± 6.0^a	269.7 ± 64.1^b	306.1 ± 32.2^b	145.6 ± 17.2^{ab}	465.7 ± 56.6^{bc}	637.2 ± 28.1^c
Liver	32.7 ± 8.51^a	70.0 ± 14.7^b	77.1 ± 27.4^b	84.7 ± 17.0^b	177.9 ± 34.0^{bc}	208.9 ± 26.5^c
Red blood cells	18.6 ± 3.84^a	35.8 ± 4.71^b	46.1 ± 7.57^b	30.7 ± 3.42^b	75.3 ± 15.1^{bc}	119.1 ± 17.4^c
Red muscle	5.91 ± 1.98^a	12.1 ± 3.40^b	15.7 ± 3.59^b	11.2 ± 2.99^b	29.1 ± 6.99^{bc}	47.1 ± 34.9^c
Adipose	5.13 ± 0.92^a	10.4 ± 0.86^b	13.4 ± 0.87^b	8.31 ± 0.43^{ab}	24.5 ± 1.71^{bc}	32.8 ± 1.05^c
Fillet	2.96 ± 0.97^a	5.60 ± 1.79^{ab}	7.26 ± 1.99^b	5.00 ± 0.84^b	13.81 ± 2.64^{bc}	19.5 ± 1.21^c
Bile	12.0 ± 3.2^a	17.0 ± 5.31^{ab}	14.6 ± 3.57^b	41.2 ± 8.12^c	94.9 ± 31.9^d	152.0 ± 111.8^d
Feces*	283.5 ± 46.8^a	370.8 ± 40.7^a	328.8 ± 44.7^a	248.8 ± 46.1^a	303.4 ± 60.5^a	334.3 ± 35.5^a

Values in rows with the same superscripts are not significantly different (nested one-way ANOVA, Tukey's *t*-test, *p* value).
*Data from trial day 56.

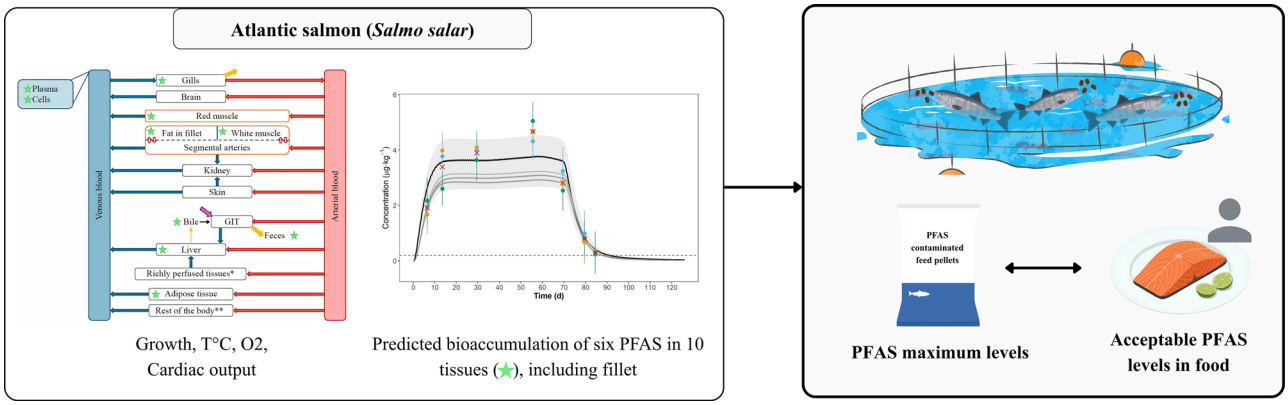

Fig. 1 | A PBK Model for PFAS Transfer from feed to fillet in farmed Atlantic salmon.

Predicted fillet concentrations for all 4-EFSA regulated PFAS remained below current European ML (ML: PFOA 0.03, PFNA 0.1, PFHxS 0.01, PFOS 2 µg/kg ww). When feed concentrations were simulated at five times the highest observed 4-EFSA levels, predicted fillet concentrations approached the ML for PFOS while remaining below the ML for the other three regulated PFAS. Feed-to-fillet transfer followed a linear relationship across all simulated exposure levels ($R^2 = 1$; Fig. S15) enabling direct determination of maximum acceptable PFAS concentrations in feed compatible with established European food safety limits. Based on the current European ML in seafood for the 4-EFSA regulated PFAS[6], the model-derived maximum acceptable feed concentrations are: 1.43 µg PFOA kg^{-1}, 2.50 µg PFNA kg^{-1}, 0.103 µg PFHxS kg^{-1}, and 11.24 µg PFOS kg^{-1} feed.

Discussion

The present study describes the PFAS-specific organ kinetics using new experimental data obtained by feeding Atlantic salmon with a diets enriched with six PFAS congeners. A PBK model was developed to characterize PFAS kinetics and the transfer of these compounds from fish feeds to the fillet of farmed Atlantic salmon. The model allows prediction of acceptable salmon feed PFAS levels based on established PFAS seafood safety limits under different exposure and farming scenarios.

These results complement and extend existing knowledge on PFAS toxicokinetics derived from other PFAS compounds and from studies conducted in different species. In addition, this study highlight key areas where the model could be further refined, and carries important implications for the interpretation and derivation of regulatory PFAS limit values in animal feed.

The tissue distribution of PFAS observed in the present study is consistent with the known proteinophilic behavior of PFAS, which contrasts markedly with the lipophilic behavior of other persistent organic pollutants such as polychlorinated biphenyls[38]. The preferential accumulation in blood plasma reflects well-documented albumin-binding affinity[18,39], resulting in elevated plasma concentrations relative to adipose and muscle tissues. This pattern is consistent with findings in terrestrial food-producing animals: cattle exhibited lower PFAS concentrations in meat compared to blood[34], and in swine, PFOS concentrations in muscle were an order of magnitude lower than in liver[18,40].

The congener-specific differences in fillet accumulation (Fig. 4)—with sulfonic acids accumulating more than carboxylic acids of equivalent chain length—are in agreement with patterns previously reported in other fish species[22,23] and in farmed land animals[18,19]. The nearly threefold higher accumulation of PFOS over PFNA, and sevenfold over PFOA, despite all three sharing an eight-carbon backbone, underscores the independent role of the functional group in governing tissue partitioning. By contrast, PFOA and PFOS concentrations in pork muscle were reported at similar levels[40], suggesting species-specific differences in the relative influence of functional group on accumulation. The similar accumulation of PFBS and PFOA, despite PFBS having a shorter carbon chain, further confirms that functional group effects can counteract expected chain length-driven bioaccumulation patterns, consistent with observations in cattle[18,34]. This has practical implications for contaminant risk assessment: the assumption that short-chain PFAS replacing long-chain compounds carry uniformly lower bioaccumulation risk may not hold across species or functional groups. Future research should assess the effects of isomeric structure—particularly

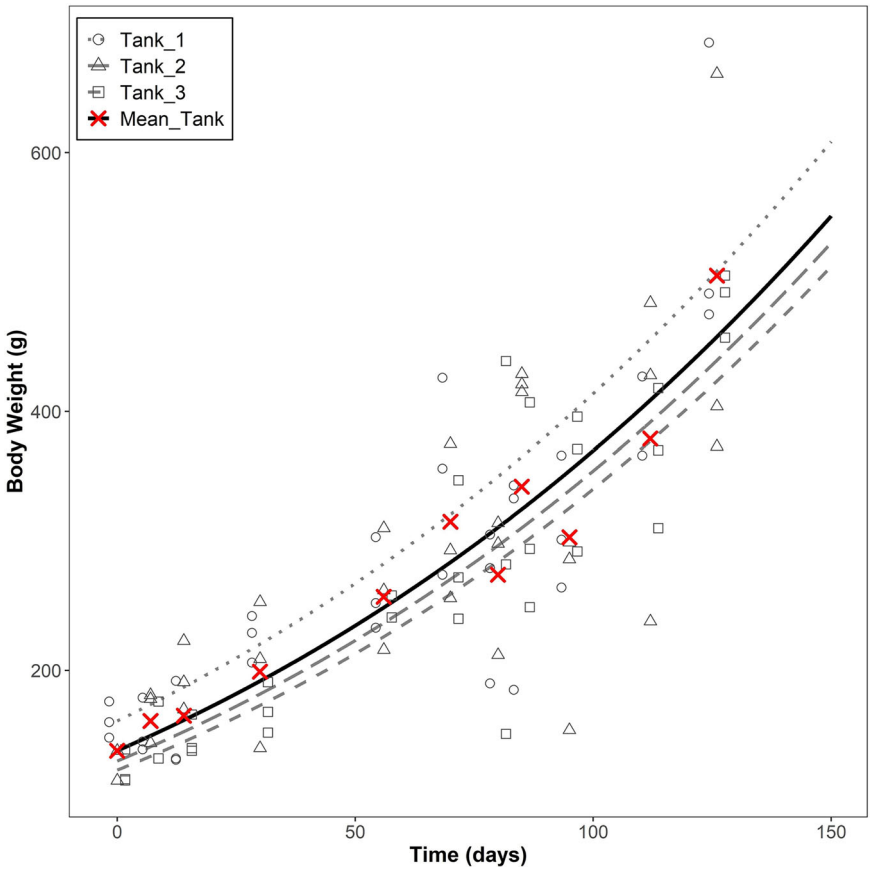

Fig. 2 | Mean growth trajectory prediction of smolt Atlantic salmon by the DEB model. Each line represents a DEB model prediction, while the symbols (cross, triangle, circle, square) represent measured experimental data. The solid line with red crosses shows the mean body weight across the three tanks; the dotted line with circles represents tank 1; the long-dashed line with triangles represents tank 2; and the short-dashed line with squares represents tank 3.

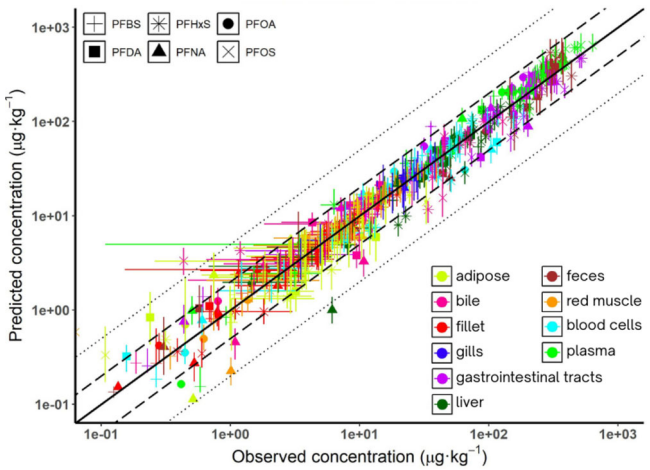

Fig. 3 | Calibration assessment: comparison of measured concentrations and model simulations for all six PFAS. The solid line corresponds to the identity line, the dashed line to the twofold range, and the dotted line to the fivefold range.

the degree of carbon chain branching—on PFAS kinetics and their implementation in PBK models, as isomeric differences are known to influence accumulation in rainbow trout[41] but were beyond the scope of the present study.

The accurate reproduction of Atlantic salmon growth trajectories by the DEB sub-model was essential to the reliability of tissue concentration predictions throughout the production cycle. In open sea cage farming, fish body weight can increase several-fold, and growth dilution substantially reduces organ PFAS concentrations compared to constant-physiology models[24]. Correctly representing growth, feed intake, and fat deposition is particularly critical in feed-to-food transfer models for farmed Atlantic salmon, where physiological characteristics are strongly life-stage dependent and fat deposition is highly dynamic[29,30]. The fat fraction in the fillet varied from ~8 to 23% across the trial - a range that has a substantial direct impact on PFAS distribution between lipid and protein compartments, and which would be poorly captured by a static physiology model. This work further highlights the importance of coupling PBK models with a DEB submodel to explicitly represent growth and changing body composition in food safety assessments.

The shift in key sensitivity parameters between accumulation and depuration phases reflects the changing dominance of kinetic processes over time: oral absorption and tissue partitioning govern uptake, while branchial excretion becomes rate-limiting during elimination. The finding that $PC_{blood:water}$—which controls the concentration gradient driving branchial excretion—was among the most influential parameters yet remains experimentally poorly constrained for fish, identifies gill exchange measurements as a high-priority future experimental need for improving model reliability. The non-identifiability of PA_{fat} during the calibration step was expected, as no distinction was made between white muscle and fat fractions in fillet samples, and diffusion processes act on timescales shorter than the 156-day study duration. Identifiability of this parameter could be improved by measuring PFAS separately in the fat and protein fractions of the fillet at shorter sampling intervals, though this presents technical challenges. As PBK models are increasingly parameterized using new approach methods (NAM), the ability to predict tissue:plasma partition coefficients from molecular properties will progressively reduce dependence on calibration-based estimations.

The decreasing K_u values with increasing carbon chain length among carboxylic acids indicate that intestinal absorption is slower for more lipophilic, longer-chain analogs, rather than the converse. Critically, this means that intestinal uptake is not the driving process behind the higher fillet accumulation of longer-chain PFAS observed in this and previous

Table 2 | Calibrated parameters for carboxylic acids

	PFOA		PFNA		PFDA	
Parameters	**MPV**	**95% CI**	**MPV**	**95% CI**	**MPV**	**95% CI**
Partition coefficients organ *i*:plasma (PC_i, no unit)						
Plasma:water	234.0	[173.0; 266.4]	143.9	[114.7; 192.8]	230.6	[153.3; 255.8]
GIT	12.2	[10.3; 19.1]	11.8	[8.8; 17.0]	4.0	[3.41; 6.21]
Liver	1.2	[1.0; 1.8]	3.0	[2.4; 4.4]	2.8	[2.1; 3.8]
Adipose	0.11	[0.08; 0.34]	0.37	[0.18; 0.55]	0.22	[0.14; 0.46]
RPT	1.00×10^{-3}	$[4.2 \times 10^{-4}; 1.6 \times 10^{-3}]$	1.20×10^{-3}	$[4.2 \times 10^{-4}; 1.6 \times 10^{-3}]$	1.1×10^{-3}	$[4.1 \times 10^{-4}; 1.6 \times 10^{-3}]$
Carcass	8.50×10^{-4}	$[3.9 \times 10^{-4}; 1.6 \times 10^{-3}]$	1.10×10^{-3}	$[4.2 \times 10^{-4}; 1.6 \times 10^{-3}]$	7.9×10^{-4}	$[3.9 \times 10^{-4}; 1.6 \times 10^{-3}]$
Skin	0.33	[0.22; 0.45]	0.42	[0.30; 0.54]	0.38	[0.30; 0.54]
Gills	0.84	[0.50; 1.4]	1.3	[0.90; 3.3]	1.16	[0.99; 3.09]
RM	0.32	[0.26; 0.52]	0.76	[0.58; 0.99]	0.57	[0.56; 0.97]
WM	0.2	[0.14; 0.29]	0.38	[0.24; 0.54]	0.28	[0.24; 0.48]
Blood cells	1.5	[1.2; 2.2]	2.5	[1.9; 4.0]	2.20	[1.87; 3.61]
Brain	*0.22**	—	*0.22*	—	*0.22**	—
Kidney	*0.7**	—	*0.7*	—	*0.7**	—
Permeability coefficient (PA_i, mL/d)						
WM	16.6	[4.2; 7742.0]	12.2	[10.3; 8338.1]	52.0	[17.6; 8568.3]
Fat in fillet	2.70×10^{-12}	$[2.7 \times 10^{-12}; 3.4 \times 10^{-1}]$	1.90×10^{-5}	$[3.5 \times 10^{-3}; 3.6 \times 10^{-1}]$	1.3×10^{-6}	$[2.1 \times 10^{-6}; 3.6 \times 10^{-1}]$
Free fraction (%)						
Free	0.085	—	0.0542	—	0.0565	—
First-order kinetic constants (day^{-1})						
$K_{e,bile}$	0.59	[0.44; 0.94]	0.69	[0.40; 0.94]	0.50	[0.39; 0.83]
$K_{e,feces}$	0.25	[0.21; 0.33]	0.67	[0.30; 2.7]	0.51	[0.37; 3.88]
K_{UtoL}	5.80×10^{-3}	$[3.4 \times 10^{-3}; 4.3 \times 10^{-2}]$	8.50×10^{-3}	$[2.1 \times 10^{-3}; 2.9 \times 10^{-2}]$	2.8×10^{-3}	$[1.7 \times 10^{-3}; 2.5 \times 10^{-2}]$
K_u	0.82	[0.48; 5.7]	0.21	[0.16; 0.24]	0.17	[0.13; 0.18]

Values marked with * represent data from PFNA used for PFOA and PFDA. Values in italic are from ref. 35. Values without 95% CI correspond to fixed parameters (not calibrated).
MPV most probable value (mode of the posterior distribution), *CI* credibility interval.

studies[19,20]. Instead, differences in organ partitioning, distribution, and excretion appear to be the primary determinants of congener-specific accumulation, consistent with the strong influence of tissue:blood partition coefficients in the SA. Comparison with published K_u estimates for PFAS in fish[35] supports cross-species consistency for sulfonic acids: K_u for PFOS and PFHxS in rainbow trout were reported at 0.13 and 0.16 day^{-1}, respectively, compared to our estimates of 0.20 day^{-1} for both, suggesting similar intestinal absorption dynamics across salmonid species. For PFNA, the rainbow trout estimate of 0.08 day^{-1}[35] is lower than our estimate of 0.21 day^{-1}, a discrepancy likely reflecting differences in model structure and assumptions between studies rather than a true biological difference. The identical K_u values estimated for PFHxS and PFOS suggest that additional mechanisms not captured in the current model may influence sulfonic acid absorption kinetics, warranting further investigation.

The dominance of branchial elimination (~98% of total free PFAS excretion) was unexpected, as dietary exposure was initially hypothesized to result in predominantly fecal and biliary elimination consistent with earlier rainbow trout studies[35]. Several methodological differences likely explain this discrepancy. In the present study, feces were collected from the distal intestine, whereas ref. 35 assessed a broader section of the gastrointestinal lumen, likely capturing a larger unabsorbed PFAS fraction. Fish were also fasted for 21.5 h prior to bile sampling to allow accumulation in the gall bladder, whereas ref. 35 did not fast fish, potentially underestimating bile concentrations due to recent emptying. Finally, the higher swimming activity associated with open sea cage farming may have enhanced ventilation rate and branchial clearance relative to controlled laboratory conditions. The negligible PFAS concentrations detected in tank water throughout the experiment further support the conclusion that branchial excretion drove the observed dynamics. Together, these results suggest that under open seawater farming conditions, branchial clearance is the dominant route of PFAS depuration, with fecal and biliary routes contributing little to overall elimination. This finding has implications for model applicability: in farming systems with elevated waterborne PFAS—including recirculating aquaculture systems, stagnant pond systems, or farms near contaminated sites—branchial exchange would act simultaneously as an uptake and excretion route, and the model would require parameterization of this bidirectional flux with dedicated experimental data.

Another controversial process concerning PFAS kinetics is enterohepatic recirculation. In zebrafish (*Danio rerio*)[42], Japanese puffer fish (*Takifugu rubripes*)[43], and juvenile rainbow trout[44,45], enterohepatic recirculation has been suggested to be present and to have a strong impact on PFAS accumulation. In mammals, enterohepatic circulation is also an important mechanism for PFAS uptake and accumulation potential[38,46,47]. The absence of a detectable enterohepatic recirculation effect in our model is consistent with findings for PFOS in rainbow trout[35], and does not imply that this process is absent in Atlantic salmon. At the timescale of the present study, its kinetic signature is confounded with global absorption and excretion processes and cannot be identified from tissue concentration data alone. Disentangling this contribution will require more detailed mechanistic data, including in vitro measurements of biliary secretion and intestinal reabsorption rates. As PBK models become more mechanistic and informed by in vitro parameters, interspecies differences in enterohepatic recirculation will need to be explored experimentally, as they likely affect the overall accumulation potential of dietary PFAS.

Table 3 | Calibrated parameters for sulfonic acids

	PFBS		PFHxS		PFOS	
Parameters	**MPV**	**95% CI**	**MPV**	**95% CI**	**MPV**	**95% CI**
Partition coefficients organ *i*:plasma (PC_i, no unit)						
Plasma:water	373.1	[305.6; 516.9]	404.7	[313.0; 450.2]	310.1	[256.3; 378.3]
GIT	12.2	[10.4; 20.2]	10.2	[8.9; 15.4]	5.9	[5.1; 9.1]
Liver	2.1	[1.5; 2.9]	3.6	[2.8; 4.6]	4.2	[3.0; 5.3]
Adipose	0.20	[0.10; 0.41]	0.44	[0.24; 0.77]	0.36	[0.25; 0.74]
RPT	6.9×10^{-4}	[4.1×10^{-4}; 1.6×10^{-3}]	1.1×10^{-3}	[4.1×10^{-4}; 1.6×10^{-3}]	1.0×10^{-3}	[4.2×10^{-4}; 1.6×10^{-3}]
Carcass	1.2×10^{-3}	[4.2×10^{-4}; 1.6×10^{-3}]	9.4×10^{-4}	[4.3×10^{-4}; 1.6×10^{-3}]	1.0×10^{-3}	[4.2×10^{-4}; 1.6×10^{-3}]
Skin	0.38	[0.26; 0.51]	0.46	[0.35; 0.60]	0.47	[0.33; 0.57]
Gills	0.85	[0.41; 1.4]	1.6	[0.87; 2.4]	0.92	[0.61; 0.99]
RM	0.45	[0.25; 0.52]	0.71	[0.59; 0.97]	0.80	[0.65; 0.99]
WM	0.26	[0.14; 0.33]	0.32	[0.28; 0.51]	0.55	[0.35; 0.73]
Blood cells	1.7	[1.3; 2.6]	2.6	[2.1; 3.7]	3.0	[2.4; 4.5]
Brain	*0.64**	—	*0.37*	—	*0.64*	—
Kidney	*0.60**	—	*0.55*	—	*0.60*	—
Permeability coefficient (PA_i, mL/d)						
WM	6.6	[3.7; 7141.4]	26.4	[28.1; 8773.1]	39.5	[23.6; 8593.4]
Fat in fillet	0	[7.3×10^{-10}; 4.9×10^{-5}]	0	[1.8×10^{-11}; 9.2×10^{-1}]	1.9×10^{-6}	[1.9×10^{-6}; 5.0×10^{-1}]
Free fraction (%)						
Free	0.1125	—	0.0630	—	0.0518	—
First-order kinetic constants (day^{-1})						
$K_{e,bile}$	0.82	[0.52; 1.2]	1.0	[0.89; 1.6]	1.0	[0.83; 1.7]
$K_{e,feces}$	0.23	[0.19; 0.25]	0.14	[0.12; 0.22]	0.15	[0.14; 0.27]
K_{UtoL}	2.70×10^{-3}	[2.6×10^{-3}; 1.0×10^{-1}]	1.4×10^{-3}	[1.0×10^{-3}; 2.8×10^{-3}]	1.1×10^{-3}	[1.1×10^{-3}; 3.2×10^{-3}]
K_u	0.68	[0.74; 25.4]	0.20	[0.16; 0.27]	0.20	[0.17; 0.25]

Values marked with * represent data from PFOS used for PFBS. Values in *italic* are from ref. 35. Values without 95% CI correspond to fixed parameters (not calibrated).
MPV most probable value, *CI* credibility interval.

A central process in assessing PFAS organ kinetics in mammals[46,48,49] and fish[35,50] is the binding affinity of PFAS congeners to plasma albumin, which affects organ partitioning. The plasma PFAS that is not bound to protein is available for excretion or organ redistribution, while the bound fraction in tissues and organs is related to increased organ PFAS burdens[51]. The strong influence of the free plasma fraction in the SA, particularly for blood concentrations across both phases, reflects the fact that the model tracks free PFAS while measurements capture total (free + albumin-bound) plasma PFAS. This result is consistent with previous findings[35,50], and is expected as the model tracks free PFAS whereas plasma measurements reflect total PFAS. The actual free fraction in Atlantic salmon is difficult to measure directly. Kinetics of the binding to plasma albumin and subsequent release are not taken into account in the present model; the actual value of the free fraction is therefore unidentified from our data, and errors in this parameter could be compensated for in the estimated tissue:plasma partition coefficients. It should be noted that the tissue:plasma partition coefficients calibrated in this study represent effective parameters that implicitly incorporate plasma protein binding. Available data constrained us to set the free fraction to a fixed value, therefore the mechanistic interpretability of the estimated partition coefficients is limited due to the compromise between predictive performance and biological accuracy. Rainbow trout show near −99% plasma binding for PFOS[52], yet with lower overall binding affinity than bovine or human plasma due to higher plasma lipid levels and the lower binding capacity of fish apolipoproteins compared to serum albumin[48,53]. Consistent with these differences, the PFOS plasma half-life estimated in the present study (17–25 days) is substantially shorter than values reported in mice (31–43 days) and swine (up to 1.7 years)[18], underscoring the marked interspecies variability in PFAS kinetics that must be captured in species-specific models. Atlantic salmon are adapted for high-fat diets (>16% lipid) and efficient fatty acid transport, resulting in lipid-rich plasma that likely shifts PFAS binding toward non-specific lipid interactions rather than the albumin-dominated kinetics typical of mammals[54]. Future model refinement would benefit from direct experimental characterization of the free fraction in Atlantic salmon plasma. Equilibrium dialysis—in which plasma is separated from a buffer by a semipermeable membrane until equilibrium is reached—is the most established method for measuring unbound plasma fractions of environmental contaminants and would be directly applicable to PFAS in salmon plasma. However, as PFAS can bind to multiple plasma proteins beyond albumin, including fatty acid binding proteins and apolipoproteins, equilibrium dialysis captures total binding rather than albumin-specific affinity. A more mechanistically informative approach would be direct determination of the affinity constant (K_D) of individual PFAS congeners for Atlantic salmon albumin using radiolabelled ligand binding experiments to determine substrate-receptor affinity constants. This would allow explicit parameterization of albumin-binding kinetics and substantially improve the mechanistic interpretability of the partition coefficients in future iterations of the model.

Liver-specific binding to fatty acid binding protein (FABP) can also be incorporated in kinetic models and strongly influences liver and blood concentrations[55,56]. This mechanism was not included in the present model due to the absence of congener-specific PFAS-FABP parameters for Atlantic salmon; potential FABP binding is therefore implicitly incorporated into the calibrated liver:plasma partition coefficients. Explicit inclusion of these binding mechanisms as species-specific data become available will improve both the mechanistic interpretability and predictive accuracy of future

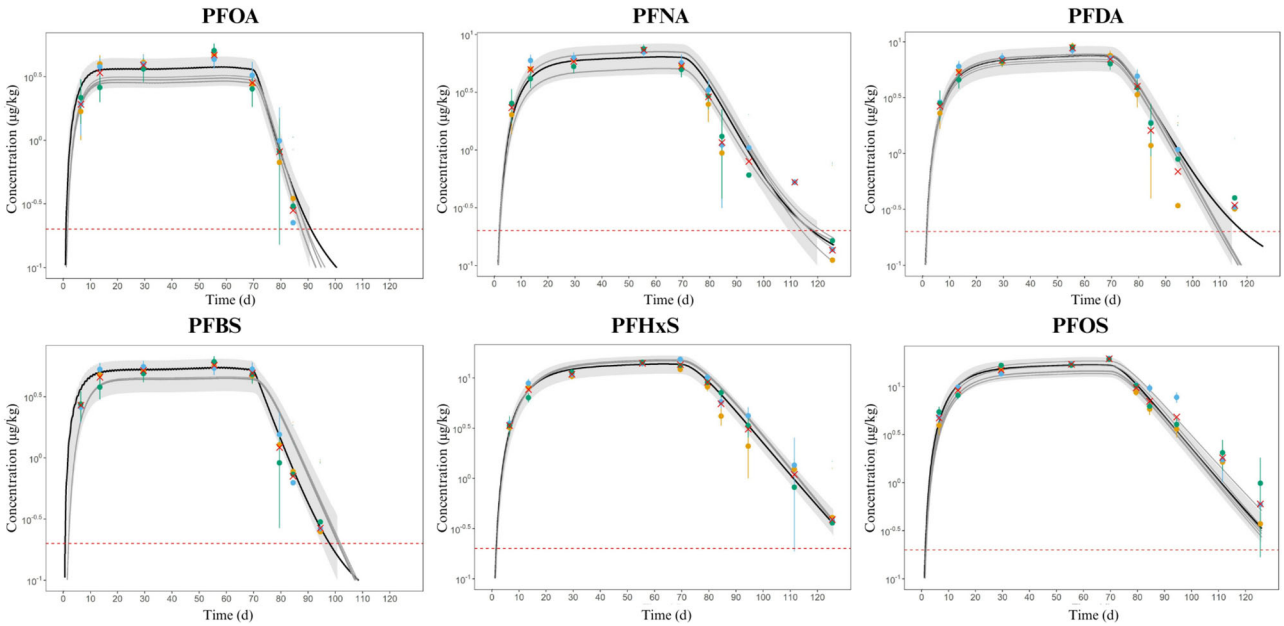

Fig. 4 | Prediction of PFAS bioaccumulation and elimination in fish fillet. PFAS concentrations (μg/kg) are shown on a $\log_{10}$ scale. Each point corresponds to one replicate (tank), and cross marks indicate the mean concentration across replicates at each sampling time. The shaded ribbon shows the 95% credible interval of the model predictions, computed from the posterior distributions, around the mean predicted concentration. The solid line represents the most probable value (MPV) of the prediction. Gray lines show the five best individual model predictions, and the red dotted line indicates zero level.

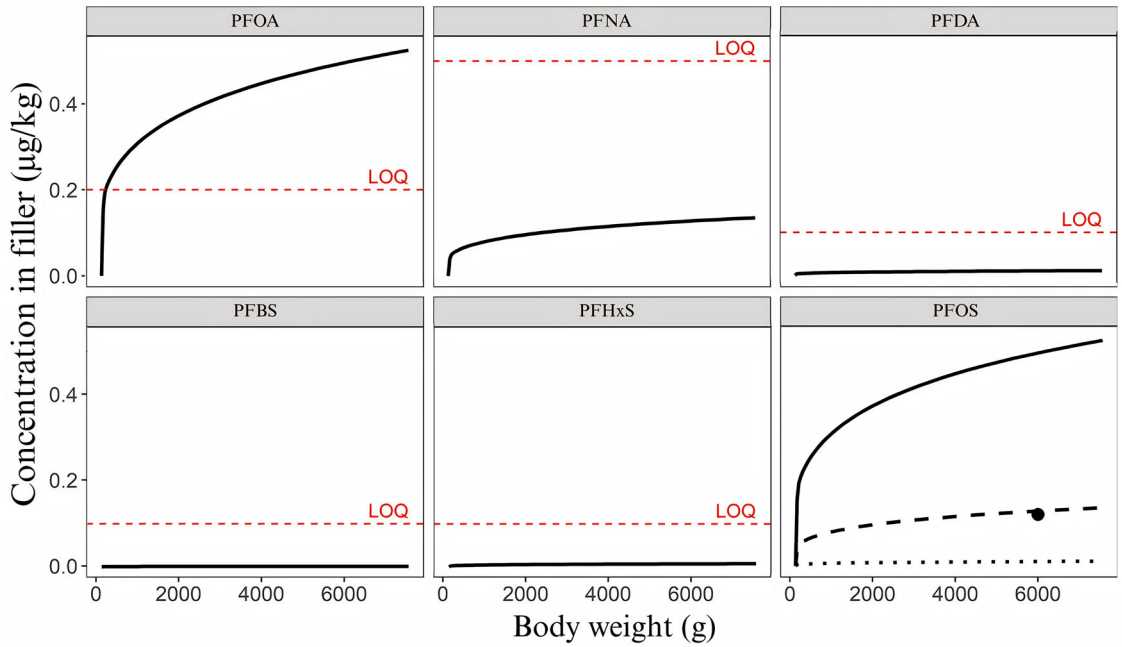

Fig. 5 | Evaluation of the model-prediction of PFAS levels measured in salmon fillet. LOQ limit of quantification. The measured point for PFOS corresponds to the mean value as described in ref. 17. All exposure scenarios were retrieved from measured concentrations in fish feed as described in ref. 17. Solid lines represent the maximum levels observed. For PFOS, the dashed line represents the mean level (0.73 µg/kg), the dotted line the minimum observed level (0.06 µg/kg), and the point represents the mean measured level in fish fillet.

models. The unique physiology of Atlantic salmon fillet—in which white muscle is not directly perfused by the venous circulation[57,58]—required explicit representation of diffusion-based transport into this compartment. At the 156-day timescale of the present study, diffusion processes were fast relative to overall kinetics, and PFAS distribution in fillet was adequately described by perfusion-based kinetics for white muscle. Nonetheless, this structural representation proved sufficient, with fillet concentrations predicted within a twofold range for 90% of PFNA measurements and 100% of PFOA, PFDA, PFBS, PFHxS, and PFOS measurements—the critical endpoint for food safety assessment.

The food safety scenario simulations should be interpreted as conservative estimates, as they exclude the standard industry practice of a 14-day starvation period prior to harvest[59]. Given that estimated fillet half-lives for the 4-EFSA PFAS range from ~5 to 10 days, this pre-harvest period would be expected to meaningfully reduce fillet concentrations in commercially slaughtered salmon, further lowering the already low predicted exposure

risk. The somewhat higher 4-EFSA PFAS levels reported in the EFSA population exposure assessment for "salmon and trout" (0.31 µg/kg ww lower bound; EFSA[4]) likely reflect contributions from rainbow trout farmed in closed freshwater systems[60], where branchial uptake of waterborne PFAS[35,61] may be substantially greater than in open sea cage Atlantic salmon farming. This interpretation is consistent with surveys showing lower PFAS levels in farmed versus wild-caught fish[37,62], and with the observation that farmed Atlantic salmon contributes among the lowest PFAS dietary burdens across all seafood categories[37]. Indeed, among seafood categories, the highest PFAS levels are consistently observed in wild-caught crustaceans and bivalves[37,62], while farmed Atlantic salmon ranks among the lowest contributors to dietary PFAS intake. A notable limitation of the present model concerns PFAS precursors, which have been detected at substantial concentrations in commercial salmon feeds, in some cases exceeding levels of known regulated PFAS[17]. As precursors can biotransform into regulated PFAS[32], they represent a potentially significant hidden source of fillet PFAS contamination not captured by the current model framework. Future work should quantify precursor pools and biotransformation kinetics in Atlantic salmon to allow their integration into feed-to-fillet transfer predictions and provide a more complete picture of dietary PFAS exposure from farmed salmon. Together, this PBK model provides a mechanistic tool to link PFAS concentrations in feed to fillet concentrations under realistic aquaculture conditions and supports scenario-based evaluations relevant for developing feed guidance values consistent with existing food ML. The linear feed-to-fillet transfer relationship ($R^2 = 1$) identified across all simulated exposure scenarios confirms the model's suitability for regulatory extrapolation across a wide range of feed contamination levels. At current commercial feed contamination levels, farmed Atlantic salmon poses a low dietary PFAS exposure risk—a conclusion that holds even under worst-case modeling assumptions. As regulatory pressure to establish ML for PFAS in fish feed intensifies, species-specific, mechanistically grounded tools of the kind presented here will be indispensable for setting evidence-based thresholds that protect both consumers and the aquaculture industry.

Methods

All original data generated in this study are available at the Zenodo repository: https://doi.org/10.5281/zenodo.17868902.

Feed preparation

In total, six different PFAS were added to the feed. PFBS (≥99.0%; CAS 375-73-5), PFOA (95%; CAS 335-6-1), PFNA (97%; CAS 375-95-1) and PFDA (98%; CAS 335-76-2) were obtained from Merck (Oslo, Norway) and PFHxS (potassium salt; CAS 355-46-4) and PFOS (technical isomer mixture; 94.6%; CAS 1763-23-1) were purchased from Chiron AS (Trondheim, Norway). PFAS-spiked diets were prepared by dispersing PFAS (in crystalline form) in aquafeed-graded rapeseed oil by stirring overnight, followed by rapid shaking for 2 h. The spiked oil was used to vacuum-coat basal diets (3-mm pellets; soybean concentrate 33%, wheat gluten 14%, fish meal 15%, wheat 6%, fava beans 4%, rapeseed oil 2%, fish oil 4%, vitamin and mineral mix 3%) at 13% rapeseed oil and 6% fish oil inclusion level. The basal feed composition and feed ingredients were chosen to minimize background levels of PFAS. The feed for the acclimation and depuration periods was prepared similarly with unspiked rapeseed oil. The final spiked concentrations in the feed were measured with averages of 410 ng g^{-1} for PFOA, 415 ng g^{-1} for PFNA, 420 ng g^{-1} for PFDA, 350 ng g^{-1} for PFBS, 340 ng g^{-1} for PFHxS, and 230 ng g^{-1} for PFOS. Background PFAS levels in the basal feed were accounted for in the analysis by maintaining a control group of fish fed the unspiked basal diet throughout the entire trial duration. Dose correction was subsequently applied to all measured tissue concentrations using the measured spiked concentrations in feed, with the highest PFAS concentration measured (PFDA) defined as one and concentrations of the other PFAS defined in relation to that. Dose correction factors and calculations are given in the Excel file available at the Zenodo repository. The final feed was stored at −20 °C until use.

Feeding trial and sampling

A feeding trial with locally bred seawater-adapted post-smolt Atlantic salmon (*Aquagen* strain) was conducted at the aquaculture station of the Institute of Marine Research in Matre (Western Norway) from 26 February to 1 July 2024. The trial was conducted in accordance with EC Directive 86/609/EEC and Norwegian regulation on animal experiments. The experimental design was approved by the Norwegian Food Safety Authorities prior to the experiment (FOTS ID 30521). Salmon with average (±SD) initial weight and length of 138 ± 21 g and 22.1 ± 1.5 cm, respectively, were kept in four 500-L fiberglass flow-through tanks with 45 fish each and were acclimated for four weeks. During the acclimation period, all fish were fed a PFAS-free control diet. Afterward, fish in three tanks were fed with the PFAS-enriched diet for 70 days, followed by a depuration phase of 56 days, while fish in the fourth tank were fed clean feed throughout. Fish were fed twice a day under an ad libitum feeding regime, with overfeeding, at ~2.4 and 1.1% of body weight at the beginning and end of the exposure period, respectively. Non-eaten feed was collected within 1 h after feeding to assess feed intake per tank. Water temperature, salinity, and oxygen content (measured at outlet) were 10 °C, 2.5%, and >80%, respectively, throughout the trial. Possible leakage of PFAS from feed and feces to the water was minimized by a high-flow conical-shaped tank design, ensuring rapid drainage of fine solids. Water samples were taken after feeding, and no detectable PFAS levels were observed (LOQ of 0.1 µg L^{-1}, data not shown).

On days 0, 7, 14, 30, 56, 70, 80, 85, 95, 112, and 126, nine fish (three per tank) were terminally anesthetized with an overdose of Tricaine MS-222 (Pharmaq; ~40 mg L^{-1}). Tables S1 and S2 in the Supporting Information (SI) give an overview of the physiological data of the fish and types of samples collected per time point, respectively. Ten different tissue types were collected: blood, liver, gut, adipose tissue from the belly fat, gills, bile, feces corresponding to the lumen content of the lower intestine, and a whole fillet on one side and red muscle on the other side. Blood was collected in heparinized syringes and centrifuged at 1300 rcf for 2.5 min to separately collect plasma and blood cell pellets. Samples were stored at −20 °C until further processing.

Extraction and analysis

All analytical standard mixes, native, internal standard, and recovery standard were obtained from Wellington Laboratories (Canada). PFAC-MXC (>98%) was used as a native standard and MPFAC-C-ES and MPFAC-C-IS as internal and recovery standards, respectively, both with chemical purity >98% and isotopic purity >99%. A full list of compounds is included in the SI (Table S3). Prior to extraction, the guts were emptied of all contents, and liver, muscle, adipose, and gut samples were homogenized. For gill samples, the gill arch was removed. For each batch of samples, matrix blanks containing tissue material from control tank fish and a solvent blank were prepared alongside the samples. Matrix blanks were spiked with internal standards, recovery standards, and 5 ng native PFAS standard to assess matrix effects and extraction efficiency.

Muscle samples were extracted by ultrasonication. Approximately 1 g of muscle tissue was spiked with 5 ng internal standard, and 4 mL methanol (≥99.9%; Riedel-de Haën) was added. Samples were shaken for 15 min and sonicated for 60 min, followed by centrifugation for 10 min at 4000 rpm. The supernatant was filtered through a 0.45- µm Millex syringe filter (nylon, 33-mm diameter; Merck Millipore), diluted with 32 mL of Milli-Q water, and split into two. Clean-up was performed on an ASPEC GX-274 automated solid phase extraction (SPE) system (Gilson, Middleton, WI, USA) equipped with an Oasis WAX cartridge (60 mg sorbent, 3 mL; Waters, Milford, MA, USA). The column was conditioned with 5 mL of 1% (v/v) ammonium hydroxide (25%; Merck KGaA) in methanol, 5 mL methanol, and 5 mL Milli-Q water, then washed with 5 mL of 2% (v/v) formic acid (≥98%; Supelco) in Milli-Q water prior to sample loading. Elution was performed with 1 mL of 1% (v/v) ammonium hydroxide in methanol. Recovery standards (5 ng) were added before storage at −20 °C until analysis.

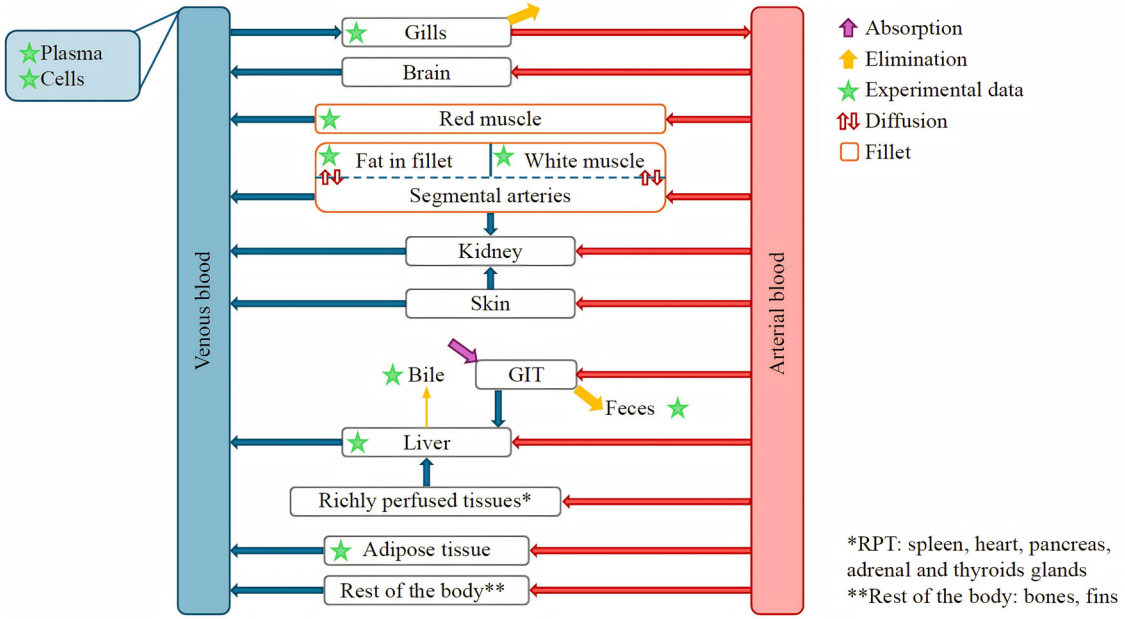

Fig. 6 | Schema of the farmed Atlantic salmon PBK model. The model consists of 15 compartments connected by arterial and venous blood circulation. The fillet is represented as three sub-compartments (red muscle, white muscle, and adipose tissue in fillet). Oral absorption through the gastrointestinal tract (GIT) is the sole exposure route modeled.

Liver, adipose tissue, gut, plasma, blood, bile, feces, and gills were extracted using a modified QuEChERS approach. Approximately 1 g of tissue was transferred to a 50 mL polypropylene centrifuge tube and spiked with 5 ng internal standard. Samples were diluted with 5 mL Milli-Q water, followed by the addition of 10 mL of 1% (v/v) formic acid (≥98%; Merck KGaA) in acetonitrile (99.99% purity for liver and adipose, VWR International; 100% purity for all other tissues, Fisher Scientific). Tubes were vortexed and sonicated for 30 min, after which the contents of a Supel QuE non-buffered Tube 2 (Sigma-Aldrich) were added, followed by immediate shaking and vortexing for at least 1 min. Samples were centrifuged at 3000 rpm at −9 °C for 10 min and stored frozen for 4 h or overnight. Following a second centrifugation (3000 rpm, −9 °C, 3 min), 5 mL of the supernatant was transferred to a Supel QuE PSA/ENVI-Carb Tube 3 (Sigma-Aldrich), shaken, vortexed, and centrifuged (3000 rpm, room temperature, 3 min). For most tissues, 1 mL of the final supernatant was transferred to LC-MS vials and spiked with 0.5 ng recovery standard. For gill samples, which were low in mass (average 0.24 g), the entire supernatant (~4 mL) was evaporated to ~1 mL before transfer and addition of recovery standard. Samples were stored frozen until analysis.

All samples were analysed with a Vanquish Flex ultra-high-performance liquid chromatography (UHPLC) system coupled to an Orbitrap Exploris 120 high-resolution mass spectrometer (Thermo Fisher Scientific, USA) equipped with a heated electrospray ionization (H-ESI) source. Chromatographic separation was achieved using a 150 × 2.1 mm, 1.8-µm Zorbax Eclipse Plus C18 column (Agilent Technologies, Santa Clara, CA, USA) with a Hypersil GOLD C18 residue trap (50 mm × 3 mm, 1.9 µm; Thermo Fisher Scientific). The mobile phase consisted of 2 mM ammonium acetate (>99.99% purity) in Milli-Q water (aqueous phase) and 2 mM ammonium acetate in methanol (organic phase), with a flow rate of 0.2 mL min^{-1}. The column and autosampler temperatures were 60 and 4 °C, respectively. The injection volume and total runtime were 5 µL and 23 min, respectively. Detailed LC and MS parameters, including the gradient program, are provided in Tables S4–S6.

PBK model structure

The PBK model was based on a generic PBK model previously applied for PFOS in rainbow trout[24,35]. Several physiological parameters and processes were adapted or added to account for the specific eco-physiology of farmed Atlantic salmon, including increasing relative fat volume (and, to a lesser extent, fillet volume) with fish size, and higher oxygen consumption in open sea cages.

The PBK model for farmed Atlantic salmon (Fig. 6) consists of 15 compartments: arterial and venous blood, gills, brain, kidney, skin, gastrointestinal tract (GIT) separated into two subsections (upper and lower intestine), liver, adipose tissue, richly perfused tissues (RPT: spleen, heart, pancreas), poorly perfused tissues (PPT: bones, fins), segmental arteries from fillet, and fillet separated into three sub-compartments: red muscle (RM), white muscle (WM), and adipose tissue in fillet. The gonads were not considered because the PBK model was developed on experimental data from sexually immature smolt fish. As this model aims to study contamination through fish feed, only oral absorption of PFAS through the GIT was considered (Fig. 7). Equation (1) describes the specific feeding quantity and thus the quantity of PFAS arriving in the upper GIT lumen:

$$\frac{d(Q_{\mathrm{admin,GIT}})}{dt} = \frac{\mathrm{DailyIntakeRate} \times BW \times C_{\mathrm{feed}}}{2 \times \mathrm{FeedingPeriod}} \quad (1)$$

where $Q_{\mathrm{admin,GIT}}$ is the quantity of each PFAS arriving in the upper GIT lumen (µg), Daily intake rate is the percentage of feed intake per body weight per day (%), BW is the body weight (g), C_{feed} is the concentration of each PFAS in the feed (µg g^{-1}), and feeding period is the feeding window duration (d).

All compartments were assumed well-mixed with a blood flow-limited distribution, with the exception of the white muscle and adipose tissue in the fillet (detailed below). This assumption is standard practice in PBK modeling for ionogenic compounds in fish[24] and holds when membrane permeability is high relative to blood flow, which is generally valid for well-perfused tissues such as liver, kidney, gills, and GIT. Blood flow to tissues was calculated considering the free fraction of each PFAS in plasma (detailed in the PFAS-specific parameters section) following Equation (2), as

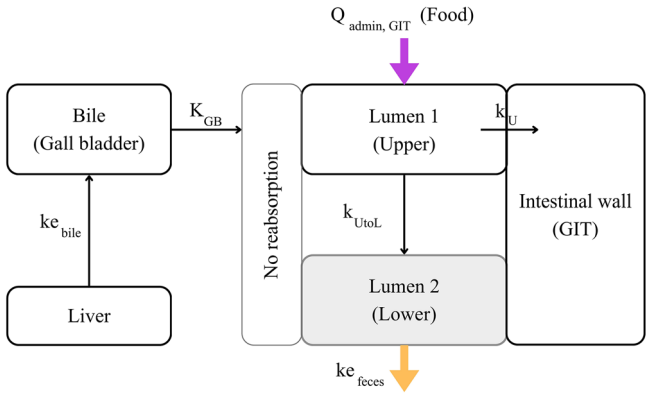

Fig. 7 | PFAS absorption and elimination through the gastrointestinal tract (GIT). The GIT lumen is divided into an upper intestine (stomach, pyloric ceca, upper intestine) and a lower intestine. PFAS transfer between compartments is regulated by the rate constants K_{UtoL}, K_u, $K_{e,feces}$, and $K_{e,bile}$.

proposed byVidal et al.[35]:

$$\frac{d(Q_i)}{dt} = F_i \times \text{Free} \times \left(C_{\text{art,plasma}}(t) - \frac{C_{\text{ven},i}(t)}{PC_i} \right) \quad (2)$$

where Q_i is the quantity of chemical in compartment i (µg), F_i is the arterial plasmatic blood flow to compartment i (mL day^{-1}), Free is the free fraction of PFAS in plasma (%), $C_{\text{art,plasma}}$ is the plasmatic arterial PFAS concentration (µg mL^{-1}), $C_{\text{ven},i}$ is the plasmatic venous blood PFAS concentration leaving compartment i (µg mL^{-1}), and t is time (day).

No hepatic metabolism was considered, as no PFAS metabolism has been documented in fish. Bile was synthesized in the liver and either accumulated in the gall bladder during fasting or was instantly released and subsequently eliminated from the GIT lumen (Fig. 7). Elimination of PFAS also occurs through branchial excretion. All model equations and source codes are available under the Zenodo DOI provided in the Software section.

Growth sub-model of farmed Atlantic salmon

The PBK model includes a growth sub-model based on DEB theory[63], driven by temperature and feeding level, as proposed in ref. 24. DEB model parameters are species-specific. The feeding level f was modeled with a hyperbolic functional response (Equation (3)) as suggested by Kooijman[63] for a given individual fish:

$$f = \frac{x}{1+x} \text{ with } x = \frac{A_{\text{feed}}}{K},\ A_{\text{feed}} = \text{DailyIntakeRate} \times BW,\ K = \frac{\varphi \times L^2}{2},\ \varphi = \frac{\dot{P}_{Am}}{k_X} \quad (3)$$

where x is the scaled food density (dimensionless), A_{feed} is the food density (J day^{-1}), DailyIntakeRate is the percentage of feed intake per body weight per day (%), BW is the body weight (g), K is the half-saturation coefficient (J day^{-1}), φ is the amount of food required for ad libitum feeding (J mm^{-2} day^{-1}), L is the structural length (mm), k_X is the conversion efficiency of food into assimilated energy, and $\dot{P}_{Am}$ is the maximum area-specific assimilation rate (J mm^{-2} day^{-1}). Growth in length was modeled using Equation (4):

$$\frac{d(L)}{dt} = \frac{\dot{v}}{3 \times (f+g)} \times \left(M \times f - \frac{L}{L_m} \right) \quad (4)$$

where $\dot{v}$ is the energy conductance (mm day^{-1}), f is the feeding level (dimensionless), g is the energy investment ratio, L is the structural length (mm), and L_m is the maximum structural length (mm). Growth trajectories from the calibration datasets were reconstructed from reported specific growth rate (SGR) and feed conversion ratio (FCR) values following:

$$\text{SGR} = 100 \times \frac{\ln W_2 - \ln W_1}{t_2 - t_1} \quad (5)$$

$$\text{FCR} = \frac{A_{\text{feed}}}{W_2 - W_1} \quad (6)$$

where W_1 and W_2 are body weights (g) at times t_1 and t_2 (days), and A_{feed} is feed intake (g).

Physiological processes specific to Atlantic salmon

Cardiac output (F_{card}, mL day^{-1}), depending on both water temperature and fish mass, was implemented integrating an Arrhenius temperature correction and the free fraction of PFAS in plasma (Equations (7–8)), as proposed by ref. 24:

$$F_{\text{card,g}} = F_{\text{card,ref}} \times e^{\left(\frac{T_A}{T_R} - \frac{T_A}{T_K}\right)} \times \left(\frac{BW}{BW_{F_{\text{card,ref}}}} \right)^{-0.1} \quad (7)$$

$$F_{\text{card}} = F_{\text{card,g}} \times BW \times \text{Free} \quad (8)$$

where $F_{\text{card,g}}$ is the mass-specific cardiac output (mL day^{-1} g^{-1}), $F_{\text{card,ref}}$ is the reference cardiac output (mL day^{-1} g^{-1}), T_A is the Arrhenius temperature (°K), T_R is the reference temperature (°K), T_K is the water temperature (°K), BW is the body weight (g), $BW_{F_{\text{card,ref}}}$ is the reference body weight at which $F_{\text{card,ref}}$ was recorded (g), and Free is the plasmatic free fraction of PFAS (%). The initial Arrhenius temperature estimated for rainbow trout (T_A = 6930 °K[24]) was refitted for Atlantic salmon using R's `nls` function (`nlstools` package, CRAN) based on experimental data from Porter and Gamperl[64] (Table S7), yielding T_A = 2545 ± 1521 °K (SE; $p < 0.236$) (Fig. S1).

Oxygen consumption rate ($\dot{V}_{O_2}$, mg g^{-1} day^{-1}) was implemented following Equation (9), as proposed by ref. 65 for Atlantic salmon, which includes body weight (BW, g), temperature (T, °C), and swimming speed (U, day^{-1}) set to 0.5, corresponding to rearing tank activity:

$$\dot{V}_{O_2} = 61.6 \times BW^{-0.33} \times 1.03^T \times 1.79^U \quad (9)$$

As adipose tissue development in fillet from smolt to adult Atlantic salmon is not linearly proportional to body weight growth, a log-linear regression (R's `lm` function, `lmerTest` package, CRAN) was performed to establish the equation of adipose tissue growth (Equation (10); R^2 = 0.71), using biometric data from this study and data from the literature[66,67] (Table S8). The relationship between the fat fraction of the fillet ($sc_{\text{fat fillet}}$, dimensionless) and body weight (BW, g), from 0.1 kg smolt to 5 kg adult fish, is:

$$sc_{\text{fatfillet}} = -0.0588 + 0.0187 \times \log(BW) \quad (10)$$

In the present study, the fat fraction in fillet represented 8.1 ± 1.6% (mean ± SD) at the start of the trial. Based on total fillet weight, the volume of the fat fraction in the fillet was estimated at each time point throughout the production cycle.

Experimental studies in Atlantic salmon showed that white muscle blood flow remains relatively constant between resting and active states, suggesting that substance distribution is not blood flow-limited in this compartment[57]. Thus, a diffusion-limited transport mechanism was modeled through the fat and white muscle of the fillet, since both tissues can hardly be separated experimentally, in contrast to the red muscle. As proposed by ref. 68 for humans, the fat and white muscle in fillet were subdivided into a vascularised compartment and an intracellular space (Fig. 6). The vascular space volume was estimated by assuming that capillaries cover 5% of the fillet surface[69,70] and applying this proportion to the combined volume of white muscle and fat in the fillet. The exchanges between the two

Table 4 | Atlantic salmon physiological parameters used in the PBK model

Definition	Parameter	Value	References
Relative weight (dimensionless)			
Blood	sc_blood	**0.059**	—
Brain	sc_brain	0.0045	24
Liver	sc_liver	**0.012**	—
Adipose tissue	sc_adipose	**0.078**	—
Skin	sc_skin	0.1	24
GIT	sc_GIT	**0.063**	—
Kidney	sc_kidney	0.0076	24
Richly perfused	sc_rp	**0.021**	—
Gills	sc_gills	**0.0049**	—
Upper intestine	sc_lumen_GIT_1	0.011	24,71
Lower intestine	sc_lumen_GIT_2	0.0013	71
White muscle	sc_WM_fillet	**0.48**	—
Red muscle	sc_RM_fillet	**0.027**	—
Fat in fillet	sc_fat_fillet	Eq. (10)	—
Poorly perfused	sc_pp	$1 - \sum sc_i$	—
Capillaries (fillet surface)	BV_fillet	0.05	69,70
Relative blood flow (dimensionless)			
Brain	frac_brain	0.018	24
Liver	frac_liver	0.016	24
Adipose tissue	frac_adipose	0.0058	24
Skin	frac_skin	0.057	24
GIT	frac_GIT	0.49	24
Kidney	frac_kidney	0.082	24
Richly perfused	frac_rp	0.094	24
Gills	frac_gills	0.0021	35,80
Fillet (vascular)	frac_fillet	0.16	57
Red muscle	frac_RM_fillet	0.001	57
Poorly perfused	frac_pp	$1 - \sum frac_i$	—
Fillet blood flow to kidney	aF_fillet	0.4	24
Skin blood flow to kidney	aF_skin	0.1	24
Cardiac output and respiratory parameters			
Arrhenius temperature (°K)	TA_Fcard	**2545**	—
Optimal temperature (°K)	TR_Fcard	281.15	64
Reference cardiac output (mL day^{-1} g^{-1})	F_card_ref	56.84	64
Effective respiratory volume (mL day^{-1})	$\dot{V}_{O_2}$	Eq. (9)	24

Values in bold are specific to Atlantic salmon measured in this study. All remaining values are from rainbow trout.

sub-compartments are governed by a permeability coefficient (PA, mL day^{-1}). In the white muscle and fat compartment of the fillet ($i \in$ {fat fillet, WM fillet}), the quantities in the vascular ($Q_{\text{fillet blood}}$, μg) and intracellular spaces (Q_i, μg) are respectively:

$$\frac{d(Q_{\text{filletblood}})}{dt} = F_{\text{fillet}} \times \text{Free} \times \left(C_{\text{art,plasma}}(t) - C_{\text{filletblood}}(t)\right) - \sum_i \frac{d(Q_i)}{dt} \quad (11)$$

$$\frac{dQ_i}{dt} = PA_i \times \left(C_{\text{filletblood}}(t) - \frac{C_i(t)}{PC_i}\right) \quad (12)$$

Parameterization of the PBK model

The PBK model was parameterized using two categories of input: (i) physiological parameters specific to Atlantic salmon, and (ii) PFAS-specific biochemical parameters.

The physiological parameters for Atlantic salmon were obtained from data generated in this experiment and from published literature. These parameters include tissue volumes, cardiac output, oxygen consumption, and blood flows, and are summarized in Table 4. Briefly, most tissue volumes were obtained from experimental data collected in this study; the remaining physiological parameters were retrieved from rainbow trout as proposed by refs. 24,57.

PFAS-specific parameters describe the absorption, distribution, and elimination of each congener and were derived as follows. Although branchial absorption and excretion pathways were included in the model, absorption and elimination processes were modeled with most precision in the GIT, as only oral exposure via feed was studied, using four first-order rate constants: $K_{\text{e,bile}}$, $K_{\text{e,feces}}$, K_{UtoL}, and K_{u} (Fig. 7). The GIT lumen was divided into two compartments: (i) an "upper intestine" comprising the stomach, pyloric ceca, and upper intestine[71], and (ii) a "lower intestine" from which feces samples were collected, corresponding to the lumen content. PFAS transfer from the upper to the lower intestine was regulated by K_{UtoL}. Throughout the upper intestine, PFAS absorption from the lumen to the GIT wall occurred at a rate K_{u}. Finally, elimination from the lower intestine to the environment proceeded with a rate $K_{\text{e,feces}}$, as proposed by Nichols et al.[71] (Fig. 7).

In addition to kinetic rate constants, organ:blood partition coefficients and the free fraction in blood (Free, i.e., the fraction of PFAS not bound to albumin) were included as distribution parameters. The free fraction was estimated based on the dissociation equilibrium constant (K_{D}, mol L^{-1}) of each PFAS to Atlantic salmon albumin (Alb2-Q03156-Ssalar) using SwissDock[72,73], which estimates the Gibbs free energy (ΔG, kcal mol^{-1}) of binding using the attracting cavities option with three random initial conditions (RIC). The most negative SwissParam score (ΔG), corresponding to the strongest binding interaction, was selected for each PFAS congener (Table S9). The free fraction was obtained using Equations (13) and (14), derived from the following rationale. Total plasma PFAS is partitioned between free and albumin-bound fractions: $[\text{PFAS}]_{\text{total}} = [\text{PFAS}]_{\text{free}} + [\text{PFAS}]_{\text{bound}}$. The association constant K_A for albumin binding is defined as $K_A = [\text{PFAS}]_{\text{bound}}/([\text{PFAS}]_{\text{free}} \times [\text{Albumin}]_{\text{blood}})$. Combining these relationships and resolving for the free fraction yields Equations (13) and (14):

$$K_D = e^{\frac{\Delta G}{R \times T}} \quad (13)$$

$$\text{Free} = \frac{1}{1 + \frac{[\text{Albumin}]_{\text{blood}}}{K_D}} \quad (14)$$

where R is the universal gas constant (R = 8.314 J K^{-1} mol^{-1}), T is the reaction temperature (°K), $[\text{Albumin}]_{\text{blood}}$ is the blood concentration of albumin (mol L^{-1}), and $K_A = 1/K_{\text{D}}$.

Parameterization of the DEB sub-model

Six DEB parameters (Table 5) were calibrated using Bayesian inference from two independent literature datasets[67,74], both consisting exclusively of Atlantic salmon reared in seawater on 3-mm diameter feeds. In the ref. 74 dataset, fish were transferred from small pens to larger grow-out pens at approximately day 317, resulting in a transient reduction in growth rate (SGR = 0.94%); data were therefore split into pre- and post-transfer subsets for modeling purposes. Daily water temperatures were estimated by linear interpolation between available measurements and used as model inputs. Prior distributions of the energy investment ratio (g, dimensionless) and somatic maintenance rate coefficient (k_M, day^{-1}) were set as truncated

Table 5 | Posterior distributions of DEB parameters for Atlantic salmon (*Salmo salar*)

Parameter	δ_m	$\{\dot{P}_{Am}\}$	$\dot{v}$	$\dot{k}_M$	g	E_{Hb}	E_{Hm}	a_{bw}	b_{bw}
Unit	—	J mm^{-2} d^{-1}	mm d^{-1}	d^{-1}	—	J	J	g cm^{-1}	—
Prior	0.178	1.61	0.38	0.027	0.196	52.0	450.0	0.0051	3.35
Posterior MPV	$\approx a_{bw}^{1/3}$	1.61	0.447	6.69×10^{-3}	0.160	—	639.9	0.0036	3.34
2.5%	—	—	0.381	2.29×10^{-3}	0.109	—	511.3	0.0025	3.28
97.5%	—	—	0.491	1.30×10^{-2}	0.206	—	882.5	0.0045	3.43

MPV most probable value, *95 CI* 95% credible interval.

normal distributions. Prior distributions of energy conductance ($\dot{v}$, mm day^{-1}), energy at the state of maturity at metamorphosis (E_{Hm}, J), and the two parameters relating body weight to length (a_{bw}, g cm^{-1} and b_{bw}, dimensionless) were set to normal distributions with a 10% coefficient of variation to account for uncertainty and interindividual variability. All prior values were obtained from the add-my-pet database for rainbow trout[24]. The prediction accuracy of the calibrated DEB model for Atlantic salmon growth was assessed by comparing model predictions of body weight to the empirical biometric data collected in this study (Table S1 and Fig. 2).

PBK model calibration and validation

Model calibration and validation were performed on raw organ concentrations (i.e., not dose-corrected) using the concentration levels measured in feed for each PFAS. Based on the results of the SA, 17 parameters were calibrated using Bayesian inference for each of the six PFAS (Tables 2 and 3). Most parameters—including tissue:plasma partition coefficients, permeability coefficient (PA), and absorption and elimination constants ($K_{e,bile}$, $K_{e,feces}$, K_{UtoL}, K_u)—were assigned non-informative log-uniform prior distributions covering several orders of magnitude. Prior distributions of tissue:blood partition coefficients for the RPT and carcass (representing the rest of the body) were set to truncated normal distributions with an assumed prior mean of 10^{-3} and a 30% coefficient of variation to account for estimation uncertainty. Similarly, the prior mean of the partition coefficient for skin was based on data from rainbow trout[75] with a 30% coefficient of variation. Detailed prior distributions for each PFAS are provided in the SI (Table S11). Model calibration was evaluated using measured PFAS concentrations in each tissue sample from this study. A statistical model was used to handle censored data (i.e., values below detection limits) to maximize the information used during calibration, by allowing non-quantified levels to vary between zero and the limit of quantification[76]. Validation of the calibrated model was based on an entirely independent external dataset with no overlap with the calibration data: measured PFAS concentrations in commercial Norwegian salmon feeds[17] and corresponding fillet samples obtained through routine surveillance monitoring by the Institute of Marine Research (Table S12). This external validation dataset reflects realistic commercial aquaculture conditions and is therefore directly relevant to the regulatory application of the model.

Calibrations were performed using Bayesian methods (Monte Carlo Markov Chains, MCMC). Three independent MCMC chains were launched with 50,000 iterations each. Results were based on the last 10,000 iterations. Gelman's index was used to assess convergence ($\widehat{R} < 1.1$). Posterior distributions were used to derive the most probable value (MPV) and the corresponding 95% credible interval (95 CI) using the 2.5 and 97.5% quantiles.

Sensitivity analysis

A SA was performed using the variance-based Sobol method[77,78]. First-order and total Sobol sensitivity indices were estimated for PFOA. SA were performed at two time points representing the exposure (day 6) and depuration (day 80) phases, for concentration levels in all tissue samples collected in this study. Uniform distributions were used for 19 parameters, based on previous studies[24] and new parameters introduced in this study involved in fillet kinetics (PC_{WM_fillet}, PA_{WM}, PA_{fat}) and all parameters related to oral absorption and elimination (K_{UtoL}, K_u, Free, $K_{e,bile}$, $K_{e,feces}$). Bounds were set at ±20% of the prior mean values (Table S13).

Software

Calculations and linear regressions were performed using R Statistical Software (v4.5.1; R Core Team 2025) and GNU MCSim v6.2.0[79]. MCSim model codes are provided under https://doi.org/10.5281/zenodo.17868902 with a Creative Commons Attribution 4.0 license.

Data availability

The datasets generated and analyzed during the current study are publicly available on Zenodo under a Creative Commons Attribution 4.0 International (CC-BY 4.0) license at https://doi.org/10.5281/zenodo.17868902.

Code availability

The code used for data processing, material classification, and particle size estimation is publicly available on Zenodo at https://doi.org/10.5281/zenodo.17868902.

Received: 3 April 2026; Accepted: 15 May 2026;
Published online: 03 July 2026

References

1. Lindstrom, A., Strynar, M. & Libelo, E. Polyfluorinated compounds: past, present, and future. *Environ. Sci. Technol.* **45**, 7954–7961 (2011).
2. Ahrens, L. & Bundschuh, M. Fate and effects of poly- and perfluoroalkyl substances in the aquatic environment: a review. *Environ. Toxicol. Chem.* **33**, 1921–1929 (2014).
3. Khan, B., Burgess, R. & Cantwell, M. Occurrence and bioaccumulation patterns of per- and polyfluoroalkyl substances (PFAS) in the marine environment. *ACS EST Water* **3**, 1243–1259 (2023).
4. EFSA Risk to human health related to the presence of perfluoroalkyl substances in food. *EFSA J.* **18**, 6233 (2020).
5. Haug, L. et al. Diet and particularly seafood are major sources of perfluorinated compounds in humans. *Environ. Int.* **36**, 772–778 (2010).
6. European Commission Commission regulation (EU) 2022/2388 of 7 December 2022 amending regulation (EC) no 1881/2006 as regards maximum levels of perfluoroalkyl substances in certain foodstuffs. *Off. J. Eur. Union* **316**, 38–41 (2022).
7. European Commission Commission recommendation (EU) 2022/1431 of 24 August 2022 on the monitoring of perfluoroalkyl substances in food. *Off. J. Eur. Union* **221**, 105–109 (2022).
8. Hussey, M. et al. The relationship between PFAS exposure and dyslipidemia: an updated review, meta-analysis, and evaluation of bias. *Eur. J. Epidemiol.* **40**, 995–1029 (2025).
9. Ji, C., Pavuk, M. & Ruiz, P. Global serum per- and polyfluoroalkyl substances exposures and their correlation with lipids: a systematic review and meta-analysis. *Environ. Sci. Technol.* **59**, 19611–19629 (2025).
10. Ho, T. et al. Effects of in utero PFOS exposure on epigenetics and metabolism in mouse fetal livers. *Environ. Sci. Technol.* **57**, 14892–14903 (2023).

11. Salihovic, S. et al. Changes in markers of liver function in relation to changes in perfluoroalkyl substances–a longitudinal study. *Environ. Int.* **117**, 196–203 (2018).
12. Szilagyi, J., Avula, V. & Fry, R. Perfluoroalkyl substances (PFAS) and their effects on the placenta, pregnancy, and child development: a potential mechanistic role for placental peroxisome proliferator-activated receptors (PPARs). *Curr. Environ. Health Rep.* **7**, 222–230 (2020).
13. Abraham, K. et al. Internal exposure to perfluoroalkyl substances (pfass) and biological markers in 101 healthy 1-year-old children: associations between levels of perfluorooctanoic acid (PFOA) and vaccine response. *Arch. Toxicol.* **94**, 2131–2147 (2020).
14. European Commission. Food safety, PFAs. European Commission website (2025).
15. EFFOP. *2023 Report: Fishmeal and Fish Oil in the EU*. Tech. Rep. (European Fish Oil and Fish Meal Organization, 2023).
16. European Commission, Directorate-General for Maritime Affairs, Fisheries and EUMOFA. *The EU Fish Market – 2024 Edition*. Tech. Rep. (Publications Office of the European Union, 2024).
17. Ali, A., Berntssen, M., Sele, V. & Valdersnes, S. Wide scope screening and target quantification of per- and polyfluoroalkyl substances (PFAs) in feed and feed ingredients to farmed salmonids. *J. Hazard. Mater.* **495**, 139078 (2025).
18. Death, C. et al. Per- and polyfluoroalkyl substances (PFAS) in livestock and game species: a review. *Sci. Total Environ.* **774**, 144795 (2021).
19. Houde, M., De Silva, A., Muir, D. & Letcher, R. Monitoring of perfluorinated compounds in aquatic biota: an updated review. *Environ. Sci. Technol.* **45**, 7962–7973 (2011).
20. Kudo, N. in *Toxicological Effects of Perfluoroalkyl and Polyfluoroalkyl Substances* (ed. DeWitt, J.) Ch. 6 (Springer International Publishing, 2015).
21. Podder, A., Sadmani, A., Reinhart, D., Chang, N.-B. & Goel, R. Per and poly-fluoroalkyl substances (PFAS) as a contaminant of emerging concern in surface water: a transboundary review of their occurrences and toxicity effects. *J. Hazard. Mater.* **419**, 126361 (2021).
22. Lautz, L., Dorne, J., Oldenkamp, R., Hendriks, A. & Ragas, A. Generic physiologically based kinetic modelling for farm animals: part I. Data collection of physiological parameters in swine, cattle and sheep. *Toxicol. Lett.* **319**, 95–101 (2020).
23. Damre, A. & Banerjee, A. Beyond traditional toxicology: the transformative power of PBTK modeling. *Toxicol. Vitr.* **109**, 106111 (2025).
24. Grech, A. et al. Generic physiologically-based toxicokinetic modelling for fish: integration of environmental factors and species variability. *Sci. Total Environ.* **651**, 516–531 (2019).
25. Lautz, L., Oldenkamp, R., Dorne, J. & Ragas, A. Physiologically based kinetic models for farm animals: critical review of published models and future perspectives for their use in chemical risk assessment. *Toxicol. Vitr.* **60**, 61–70 (2019).
26. Ashauer, R. & Escher, B. Advantages of toxicokinetic and toxicodynamic modelling in aquatic ecotoxicology and risk assessment. *J. Environ. Monit.* **12**, 2056–2061 (2010).
27. Stow, C. & Carpenter, S. PCB accumulation in Lake Michigan coho and chinook salmon: individual-based models using allometric relationships. *Environ. Sci. Technol.* **28**, 1543–1549 (1994).
28. Handeland, S., Imsland, A. & Stefansson, S. The effect of temperature and fish size on growth, feed intake, food conversion efficiency and stomach evacuation rate of Atlantic salmon post-smolts. *Aquaculture* **283**, 36–42 (2008).
29. Oppedal, F., Dempster, T. & Stien, L. Environmental drivers of Atlantic salmon behaviour in sea-cages: a review. *Aquaculture* **311**, 1–18 (2011).
30. Berntssen, M., Sanden, M., Hove, H. & Lie, O. Modelling scenarios on feed-to-fillet transfer of dioxins and dioxin-like PCBs in future feeds to farmed Atlantic salmon (*Salmo salar*). *Chemosphere* **163**, 413–421 (2016).
31. Numata, J. et al. Toxicokinetics of seven perfluoroalkyl sulfonic and carboxylic acids in pigs fed a contaminated diet. *J. Agric. Food Chem.* **62**, 6861–6870 (2014).
32. Kowalczyk, J. et al. Transfer of per- and polyfluoroalkyl substances (PFAS) from feed into the eggs of laying hens. Part 2: toxicokinetic results including the role of precursors. *J. Agric. Food Chem.* **68**, 12539–12548 (2020).
33. Göckener, B. et al. Transfer of per- and polyfluoroalkyl substances (PFAS) from feed into the eggs of laying hens. Part 1: analytical results including a modified total oxidizable precursor assay. *J. Agric. Food Chem.* **68**, 12527–12538 (2020).
34. Kowalczyk, J. et al. Absorption, distribution, and milk secretion of the perfluoroalkyl acids PFBs, PFHXs, PFOs, and PFOA by dairy cows fed naturally contaminated feed. *J. Agric. Food Chem.* **61**, 2903–2912 (2013).
35. Vidal, A., Babut, M., Garric, J. & Beaudouin, R. Elucidating the fate of perfluorooctanoate sulfonate using a rainbow trout (*Oncorhynchus mykiss*) physiologically-based toxicokinetic model. *Sci. Total Environ.* **691**, 1297–1309 (2019).
36. Vidal, A., Babut, M., Garric, J. & Beaudouin, R. Temperature effect on perfluorooctane sulfonate toxicokinetics in rainbow trout (*Oncorhynchus mykiss*): exploration via a physiologically based toxicokinetic model. *Aquat. Toxicol.* **225**, 105545 (2020).
37. Marín-García, M., Fábregas, C., Argenté, C., Díaz-Ferrero, J. & Gómez-Canela, C. Accumulation and dietary risks of perfluoroalkyl substances in fish and shellfish: A market-based study in Barcelona. *Environ. Res.* **237**, 17009 (2023).
38. Zhao, M. et al. Nontarget identification of novel per- and polyfluoroalkyl substances (PFAs) in soils from an oil refinery in southwestern China: a combined approach with top assay. *Environ. Sci. Technol.* **57**, 20194–20205 (2023).
39. Lau, C. et al. Perfluoroalkyl acids: a review of monitoring and toxicological findings. *Toxicol. Sci.* **99**, 366–394 (2007).
40. Chen, W.-L., Bai, F.-Y., Chang, Y.-C., Chen, P.-C. & Chen, C.-Y. Concentrations of perfluoroalkyl substances in foods and the dietary exposure among Taiwan general population and pregnant women. *J. Food Drug Anal.* **26**, 994–1004 (2018).
41. De Silva, A., Tseng, P. & Mabury, S. Toxicokinetics of perfluorocarboxylate isomers in rainbow trout. *Environ. Toxicol. Chem.* **28**, 330–337 (2009).
42. Ulhaq, M. et al. Tissue uptake, distribution and elimination of 14C-PFOA in zebrafish (*Danio rerio*). *Aquat. Toxicol.* **163**, 148–157 (2015).
43. Honda, M. et al. High concentrations of perfluorooctane sulfonate in mucus of tiger puffer fish *Takifugu rubripes*: a laboratory exposure study. *Environ. Sci. Pollut. Res.* **25**, 1551–1558 (2018).
44. Martin, J., Mabury, S., Solomon, K. & Muir, D. Bioconcentration and tissue distribution of perfluorinated acids in rainbow trout (*Oncorhynchus mykiss*). *Environ. Toxicol. Chem.* **22**, 196–204 (2003).
45. Martin, J., Mabury, S., Solomon, K. & Muir, D. Dietary accumulation of perfluorinated acids in juvenile rainbow trout (*Oncorhynchus mykiss*). *Environ. Toxicol. Chem.* **22**, 189–195 (2003).
46. Cao, H. et al. Effect of enterohepatic circulation on the accumulation of per- and polyfluoroalkyl substances: evidence from experimental and computational studies. *Environ. Sci. Technol.* **56**, 3214–3224 (2022).
47. Wen, Y., Juhasz, A. & Cui, X. Regulating the absorption and excretion of perfluorooctane sulfonate and its alternatives through influencing enterohepatic circulation. *Sci. Total Environ.* **933**, 173161 (2024).
48. Qin, W., Escher, B., Huchthausen, J., Fu, Q. & Henneberger, L. Species difference? Bovine, trout, and human plasma protein binding of per- and polyfluoroalkyl substances. *Environ. Sci. Technol.* **58**, 9954–9966 (2024).
49. Sinclair, G. et al. Prediction of fraction unbound in human plasma for per- and polyfluoroalkyl substances: evaluating transfer learning as an algorithmic solution to the problem of sparse data. *J. Chem. Inf. Model.* **65**, 7994–8005 (2025).
50. Golosovskaia, E., Örn, S., Ahrens, L., Chelcea, I. & Andersson, P. Studying mixture effects on uptake and tissue distribution of PFAS in

zebrafish (*Danio rerio*) using physiologically based kinetic (PBK) modelling. *Sci. Total Environ.* **912**, 168738 (2024).
51. Chou, W.-C. & Lin, Z. Bayesian evaluation of a physiologically based pharmacokinetic (PBPK) model for perfluorooctane sulfonate (PFOS) to characterize the interspecies uncertainty between mice, rats, monkeys, and humans. *Environ. Int.* **129**, 408–422 (2019).
52. Consoer, D., Hoffman, A., Fitzsimmons, P., Kosian, P. & Nichols, J. Toxicokinetics of perfluorooctane sulfonate in rainbow trout (*Oncorhynchus mykiss*). *Environ. Toxicol. Chem.* **35**, 717–727 (2015).
53. Point, A. et al. Can blood proteome diversity among fish species help explain perfluoroalkyl acid trophodynamics in aquatic food webs?. *Sci. Total Environ.* **875**, 162337 (2023).
54. Torstensen, B., Nanton, D., Olsvik, P., Sundvold, H. & Stubhaug, I. Gene expression of fatty acid-binding proteins, fatty acid transport proteins (cd36 and FATP) and β-oxidation-related genes in Atlantic salmon (*Salmo salar* l.) fed fish oil or vegetable oil. *Aquac. Nutr.* **15**, 440–451 (2009).
55. Ng, C. & Hungerbühler, K. Bioconcentration of perfluorinated alkyl acids: how important is specific binding?. *Environ. Sci. Technol.* **47**, 7214–7223 (2013).
56. Mittal, V. & Ng, C. Formation of PFAAs in fish through biotransformation: a PBPK approach. *Chemosphere* **202**, 218–227 (2018).
57. Wilson, R. & Egginton, S. Assessment of maximum sustainable swimming performance in rainbow trout (*Oncorhynchus mykiss*). *J. Exp. Biol.* **192**, 299–305 (1994).
58. Stead, S. M. & Laird, L. *The Handbook Of Salmon Farming* (Springer Science & Business Media, 2002).
59. Waagbo, R., Jorgensen, S., Timmerhaus, G., Breck, O. & Olsvik, P. Short-term starvation at low temperature prior to harvest does not impact the health and acute stress response of adult Atlantic salmon. *PeerJ* **5**, e3273 (2017).
60. European Commission. Aquaculture statistics. https://ec.europa.eu/eurostat/statistics-explained/index.php?title=Aquaculture_statistics (2025).
61. Xiong, J. & Li, Z. Predicting PFAS fate in fish: assessing the roles of dietary, respiratory, and dermal uptake in bioaccumulation modeling. *Environ. Res.* **252**, 119036 (2024).
62. Zafeiraki, E. et al. Occurrence of perfluoroalkyl substances (PFASs) in a large number of wild and farmed aquatic animals collected in the Netherlands. *Chemosphere* **232**, 415–423 (2019).
63. Kooijman, B. *Dynamic Energy Budget Theory for Metabolic Organisation* 3rd edn (Cambridge Univ. Press, 2010).
64. Porter, E. & Gamperl, A. Cardiorespiratory physiology and swimming capacity of Atlantic salmon (Salmo salar) at cold temperatures. *J. Exp. Biol.* **226**, jeb245990 (2023).
65. Grøttum, J. & Sigholt, T. A model for oxygen consumption of Atlantic salmon (*Salmo salar*) based on measurements of individual fish in a tunnel respirometer. *Aquacult. Eng.* **17**, 241–251 (1998).
66. Jobling, M. & Johansen, S. Fat distribution in Atlantic salmon *Salmo salar* l. in relation to body size and feeding regime. *Aquac. Res.* **34**, 311–316 (2003).
67. Torstensen, B. et al. Tailoring of Atlantic salmon (*Salmo salar* l.) flesh lipid composition and sensory quality by replacing fish oil with a vegetable oil blend. *J. Agric. Food Chem.* **53**, 10166–10178 (2005).
68. Quindroit, P., Beaudouin, R. & Brochot, C. Estimating the cumulative human exposures to pyrethroids by combined multi-route PBPK models: application to the French population. *Toxicol. Lett.* **312**, 125–138 (2019).
69. Olsen, E. *Quantification and Characterisation of Residual Blood in Fish Muscle: Impact Of Slaughtering Methods*. Ph.D. thesis, University of Tromsø (2011).
70. Soldatov, A. Organ blood flow and vessels of microcirculatory bed in fish. *J. Evolut. Biochem. Physiol.* **42**, 243–252 (2006).
71. Nichols, J. et al. A physiologically based toxicokinetic model for dietary uptake of hydrophobic organic compounds by fish: I. feeding studies with 2,2',5,5'-tetrachlorobiphenyl. *Toxicol. Sci.* **77**, 206–218 (2004).
72. Röhrig, U., Goullieux, M., Bugnon, M. & Zoete, V. Attracting cavities 2.0: improving the flexibility and robustness for small-molecule docking. *J. Chem. Inf. Model.* **63**, 3925–3940 (2023).
73. Bugnon, M. et al. Swissdock 2024: major enhancements for small-molecule docking with attracting cavities and Autodock Vina. *Nucleic Acids Res.* **52**, W324–W332 (2024).
74. Lock, E.-J. et al. Dietary decontaminated fish oil has no negative impact on fish performance, flesh quality or production-related diseases in Atlantic salmon (*Salmo salar*). *Aquac. Nutr.* **17**, e760–e772 (2011).
75. Goeritz, I., Falk, S., Stahl, T., Schäfers, C. & Schlechtriem, C. Biomagnification and tissue distribution of perfluoroalkyl substances (PFASs) in market-size rainbow trout (*Oncorhynchus mykiss*). *Environ. Toxicol. Chem.* **32**, 2078–2088 (2013).
76. Ly, T.-K. et al. PBK-TD modelling of the gonadotropic axis: case study with two azole fungicides in female zebrafish. *Aquat. Toxicol.* **283**, 107337 (2025).
77. Martinez, J.-M. Analyse de sensibilité globale par décomposition de la variance. Presentation at GdR Ondes and GdR MASCOT-NUM, Institut Henri Poincaré, Paris, France (2011).
78. Sobol', I., Tarantola, S., Gatelli, D., Kucherenko, S. & Mauntz, W. Estimating the approximation error when fixing unessential factors in global sensitivity analysis. *Reliab. Eng. Syst. Saf.* **92**, 957–960 (2007).
79. Bois, F. GNU MCSim: Bayesian statistical inference for SBML-coded systems biology models. *Bioinformatics* **25**, 1453–1454 (2009).
80. Barron, M., Tarr, B. & Hayton, W. Temperature-dependence of cardiac output and regional blood flow in rainbow trout, *Salmo gairdneri* Richardson. *J. Fish. Biol.* **31**, 735–744 (1987).

Acknowledgements

This project was funded by the Norwegian Seafood Research Fund through the project "TRANSPFAS" (901903).

Author contributions

T.-K.L.: Conceptualization, software, methodology, visualization, formal analysis, data curation, and writing—original draft, review & editing. C.V. Data curation and writing—original draft. C.B. and R.B.: Software, supervision, and conceptualization. K.K.L.: Data curation. M.H.G.B.: Supervision, resources, project administration, funding acquisition, conceptualization, and writing—original draft, review & editing.

Funding

Open access funding provided by Institute Of Marine Research.

Competing interests

The authors declare no competing interests.

Declaration of generative AI use

During the preparation of this work, the authors used Canva to design the graphical abstract without the help of AI. Scribens was used to help with grammatical check. After using these services, the authors reviewed and edited the content as needed and took full responsibility for the content of the published article.

Additional information

Supplementary information The online version contains supplementary material available at https://doi.org/10.1038/s44454-026-00043-3.

Correspondence and requests for materials should be addressed to Rémy Beaudouin.